JGR Space Physics

RESEARCH ARTICLE
10.1029/2019JA027069

Special Section:
Equatorial Aeronomy: New results from the 15th International Symposium on Equatorial Aeronomy (ISEA-15) and beyond

Three Different Episodes of Prompt Equatorial Electric Field Perturbations Under Steady Southward IMF *Bz* During St. Patrick's Day Storm

S. Tulasi Ram[1,2], B. Nilam[2], N. Balan[1], Q. Zhang[1], K. Shiokawa[3], D. Chakrabarty[4], Z. Xing[1], K. Venkatesh[5], B. Veenadhari[2], and A. Yoshikawa[6]

[1]Institute of Space Science, Shandong University, Weihai, China, [2]Indian Institute of Geomagnetism, Navi Mumbai, India, [3]Institute of Space-Earth Environment Research, Nagoya University, Nagoya, Japan, [4]Physical Research Laboratory, Ahmedabad, India, [5]National Atmospheric Research Laboratory, Gadanki, India, [6]International Center for Space Weather Science and Education, Kyushu University, Fukuoka, Japan

Abstract Three different episodes of prompt penetration electric field (PPEF) disturbances are observed during the main phase of the St. Patrick's Day storm on 17 March 2015 under steady southward interplanetary magnetic field (IMF) *Bz* conditions unlike the conventional PPEF associated with southward or northward turnings of IMF *Bz*. These PPEF events took place during the period when strong disturbance dynamo fields are prevailing in the background. The first event is triggered by a solar wind dynamic pressure pulse that caused a sharp eastward PPEF and strong enhancement of equatorial electrojet current in Brazilian dayside. The second event caused another short but strong westward PPEF on dayside due to the reversal of IMF *By* from duskward to dawnward under steady IMF *Bz*. The third event caused a longer eastward PPEF in association with a solar wind dynamic pressure pulse followed by the onset of a substorm, which has led to strong enhancement of equatorial electrojet, quick rejuvenation and symmetric redistribution of equatorial ionization anomaly in the Brazilian sector. The signatures of the PPEF with opposite polarity and smaller magnitudes are also observed in the Asian sector on the nightside. The possible mechanisms for the observed PPEF events under steady IMF *Bz* are discussed in terms of changes in the high-latitude field-aligned currents and reconfiguration of high-latitude convection fields using Active Magnetosphere and Planetary Electrodynamics Response Experiment and Super Dual Auroral Radar Network high-frequency radar observations.

Key Points:
- Three sharp and intense PPEF disturbances under steady southward IMF Bz phase of St. Patricks's Day geomagnetic storm
- A sharp and strong westward PPEF disturbance due to sharp duskward to dawnward reversal of IMF By barring any significant change in Bz
- SW-Pdyn and Substorm induced a strong eastward PPEF, equatorial super fountain and quick rejuvenation and symmetric redistribution of EIA

Supporting Information:
- Supporting Information S1

Correspondence to:
S. Tulasi Ram,
tulasi@iigs.iigm.res.in

Citation:
Tulasi Ram, S., Nilam, B., Balan, N., Zhang, Q., Shiokawa, K., Chakrabarty, D., et al. (2019). Three different episodes of prompt equatorial electric field perturbations under steady southward IMF *Bz* during St. Patrick's Day storm. *Journal of Geophysical Research: Space Physics*, *124*. https://doi.org/10.1029/2019JA027069

Received 24 JUN 2019
Accepted 31 OCT 2019
Accepted article online 26 NOV 2019

S. Tulasi Ram is on deputation.

1. Introduction

The coupled solar wind-magnetosphere-ionosphere interactions during the disturbed space weather periods induce a variety of neutral and electrodynamic disturbances in the Earth's upper atmosphere and geomagnetic field. Several episodes of disturbances in the primary dawn-to-dusk electric field of the ionosphere were usually observed during the geomagnetic storm periods due to two key processes known as prompt penetration and ionospheric disturbance dynamo. The prompt penetration electric fields (PPEFs) due to solar wind-magnetosphere dynamo cause short-lived (~2 hr) and near simultaneous disturbances in the ionospheric electric field with the sudden changes in upstream solar wind conditions (Nishida, 1968; Senior & Blanc, 1984; Spiro et al., 1988). On the other hand, disturbance dynamo electric field (DDEF) is caused by global-scale neutral wind dynamo driven by enhanced particle and Joule heating at high latitudes (Blanc & Richmond, 1980). The DDEF in the ionosphere usually appears few hours after the onset of high-latitude auroral activity and lasts longer (several hours) (Scherliess & Fejer, 1997). Often, the electric field disturbances due to the two processes coexist and the resultant net dawn-to-dusk electric field disturbance in the ionosphere at a given instance depends on the relative magnitudes and polarities of the electric fields due to these two processes.

The electric field disturbance due to DDEF is usually westward in the dayside and eastward in the nightside, that is, opposite to the quiet time ionospheric primary dawn-to-dusk electric field. The polarity of PPEF, on the other hand, depends on the upstream solar wind conditions, primarily, on the vertical component of IMF (*Bz*). When the IMF *Bz* turns southward, the enhanced solar wind-magnetosphere interactions induce the high-latitude convection electric field via Region-1 field-aligned currents, which promptly penetrates to equatorial and low latitudes (Nishida, 1968; Senior & Blanc, 1984) through the TM0 mode propagation in the Earth-ionosphere waveguide (Kikuchi et al., 1996, 2000, 2003). The convection electric fields induce

eastward (westward) electric field perturbations in the dayside (nightside) ionosphere (Fejer & Scherliess, 1997; Kelley et al., 1979). The shielding electric fields with opposite polarity will soon develop in the inner magnetosphere in association with Region-2 field-aligned currents. The resultant PPEF disturbance in the ionospheric electric field depends on the imbalance between the convection and shielding electric fields. During southward IMF *Bz*, the convection electric field due to Region-1 currents dominates and an eastward (westward) PPEF perturbation will be observed in dayside (nightside) ionosphere. When the IMF *Bz* turns northward, the cessation of high-latitude convection leads to the domination of shielding electric fields, known as overshielding, which causes the westward (eastward) PPEF in the dayside (nightside) (Rastogi & Patel, 1975; Kikuchi et al., 1996, 2003). Kikuchi et al. (2008) have shown that the overshielding conditions may sometimes continue to dominate for about 2 hr. The effects of convection electric field in the ionosphere are usually found to be short lived (~2 hr) because of the development of counteracting shielding electric fields. However, convincing evidences have been presented for the continuous and long-duration effects of convection electric fields under steady southward IMF *Bz* conditions (Huang et al., 2005; Tulasi Ram et al., 2008).

There were other types of PPEFs reported in the recent past that do not involve any significant change in the orientation of IMF *Bz*. For example, the prompt enhancement in the eastward electric field at equatorial latitudes with the sudden increase in the solar wind dynamic pressure under steady southward or northward IMF *Bz* conditions are reported by Sastri et al. (1993), Huang et al. (2008), and Rout et al. (2016). Model simulations also reproduce such electric field changes (Lopez et al., 2004) during solar wind pressure enhancements. A few recent studies indicate that the prompt changes in the dawn-to-dusk component of the IMF (*By*) can also cause PPEF in the equatorial ionosphere (Chakrabarty et al., 2017; Kelley & Makela, 2002). Further, the PPEFs of westward polarity are observed on dayside during the onset of the substorms (Gonzales et al., 1979; Kikuchi et al., 2000, 2003; Sastri et al., 2001). On the other hand, Huang et al. (2004) and Huang (2009, 2012) has demonstrated the eastward PPEF in the dayside during the onset of sawtooth events under the steady southward IMF *Bz* periods. Recently, the eastward overshielding electric field was observed on the nightside using the high-frequency (HF) Doppler sounders, concurrently with the dayside westward equatorial electrojet (EEJ) (Hashimoto et al., 2017). However, the mechanisms responsible for the penetration of either westward or eastward electric field perturbations during the onset of substorms are not fully understood.

The St. Patrick's Day storm that occurred in the early hours of 17 March 2015 is the strongest geomagnetic storm that occurred in the Solar Cycle 24. This storm is characterized by a very long-duration main phase that lasted for nearly 17 hr, possibly, due to two successive southward IMF *Bz* structures (Kamide & Kusano, 2015). The first 8 hr of the main phase exhibited several southward and northward turnings of IMF *Bz* causing several eastward and westward PPEF events. The ionospheric response over different regions during the different phases of this storm has been extensively studied by several authors (Astafyeva et al., 2015; Batista et al., 2017; Hairston et al., 2016; Huang et al., 2016; Nava et al., 2016; Tulasi Ram et al., 2015; Venkatesh et al., 2017; Zhang et al., 2017 etc.). For example, Astafyeva et al. (2015) through global multi-instrumental observations have shown the positive ionospheric storm response at morning and postsunset local time sectors due to PPEF during the main phase. Tulasi Ram et al. (2015) have studied the equatorial electric field disturbances over Indian and Southeast Asian sectors and demonstrated the enhanced PPEF effects that are uniquely confined to narrow longitudinal sectors centered on sunset terminator. Batista et al. (2017) and Venkatesh et al. (2017) have studied the Brazilian low-latitude ionospheric response and shown the occurrence of *F*3 layer and intense equatorial ionization anomaly (EIA) during the early main phase of the St. Patrick's Day storm. The later 9 hr of the main phase is characterized by a steady southward IMF *Bz* without any orientation changes, which has led to the continuous development of ring current and intense geomagnetic storm. In this paper, we investigate the three episodes of the penetration electric field disturbances observed under this steady southward IMF *Bz* phase over Brazilian (dayside) and Southeast Asian (nightside) longitude sectors, and the effects of eastward penetration electric field occurred during a substorm on the EIA over Brazilian sector.

2. Data

The equatorial ionospheric electric field disturbances under steady southward IMF *Bz* phase of St. Patrick's day storm have been studied by using two pairs of ground based magnetometer observations from Brazilian

and Asian longitude sectors. The EEJ strength over the Brazilian sector is derived from the magnetometer measurements at an equatorial station, Belem (1.24°S, 311.73°E and 0.07°S dip latitude) and an off-equatorial station, Eusebio (3.88°S, 321.54°E and 7.63°S dip latitude). The ΔH variations at the each location were computed by removing the baseline (subtracting the average midnight values of five internationally quiet days) from horizontal (H) component of the geomagnetic field. The difference in the ΔH values between the equatorial and off-equatorial latitudes ($\Delta H_{Belem} - \Delta H_{Eusebio}$) represents the strength of EEJ and is a proxy to the equatorial zonal electric field (Anderson et al., 2002; Kane, 1974; Rastogi, 1977; Reddy, 1989 and references therein). Similarly, the EEJ strength over Asian longitudes has been computed from an equatorial and off-equatorial pair of magnetometers at Davao (7.07°N, 125.57°E and 0.2°S dip latitude) and Muntinlupa (14.34°N, 121.02°E and 8.31°N dip latitude), respectively. Further, the EIA response to PPEFs over Brazilian longitudes has been studied using ionospheric total electron content (TEC) data obtained from the madrigal database (Rudeout & Coster, 2006). The energetic electron fluxes in the kiloelectron volt range from Geostationary Operational Environmental Satellite (GOES)-15 and Van Allen Probes-A and B (formerly known as Radiation Belt Storm Probes, RBSP-A and B) were considered to examine the particle injections during the substorms. The convection map data from the Super Dual Auroral Radar Network (SuperDARN) of HF radars have been considered in this study to examine the disturbances in the high-latitude electric fields. The reduced magnetic field (H) perturbations and the derived radial currents from the Active Magnetosphere and Planetary Electrodynamics Response Experiment (AMPERE) have also been considered to investigate the changes in the high-latitude field-aligned currents during the PPEF events. Further, the interplanetary solar wind parameters observed from Wind satellite at L1 orbit, auroral, and geomagnetic activity indices such as AU, AL, and Sym-H at 1-min resolution were obtained from National Aeronautics and Space Administration's OMNI space physics data facility. The solar wind data from WIND satellite are time shifted by 50 min to account for the travel time from L1 point to bow shock nose. The shifting is done by matching the time of coronal mass ejection shock front in solar wind data with the storm sudden commencement in the H-component from the ground based magnetometers.

3. Results

A coronal mass ejection from the active Sunspot Region AR2297 on the early hours of 15 March 2015 has caused an intense geomagnetic storm on 17 March 2015, popularly known as the St. Patrick's Day storm. Figure 1 shows the UT variations of solar wind velocity, IMF *Bz*, Sym-H, and strength of EEJ derived from the two ground-based magnetometer observations over Brazilian sector on 17 March 2015. The sudden commencement of the storm has occurred around 0430 UT with the arrival of shock front as can be observed from the sudden increase in solar wind velocity, IMF *Bz*, and Sym-H index. After a brief initial phase that lasted for about 95 min, the main phase started with the southward turning of IMF *Bz* at ~0615 UT. The IMF *Bz* exhibits several northward and southward turnings between 0615 and 1415 UT. The Sym-H index also exhibited a brief recovery between 0930 and 1230 UT. The IMF *Bz* become steadily southward after 1415 UT and remained southward till 2345 UT, which has caused the continuous development of ring current and Sym-H decreased to −231 nT. Kamide and Kusano (2015) have suggested that this intense storm could have resulted from the superposition of the two successive storms driven by two successive southward IMF *Bz* structures.

3.1. PPEF Events

Figure 1d shows the EEJ variation derived from the Brazilian magnetometers on 17 March 2015, and the red curve in Figure 1d indicates the mean EEJ variation of five previous international quiet days (10th, 12th, 13th, 14th, and 15th) in the month of March 2015. The local time is approximately 3 hr 10 min behind the UT over this sector. It can be seen from this figure that the EEJ strength on 17 March significantly deviates from the quiet day mean values from the onset of main phase at 0615 UT and exhibits several negative and positive excursions with respect to its quiet day mean curve. The strong enhancement of EEJ strength between ~1200 and ~1400 UT and its impact on equatorial and low-latitude ionosphere have been thoroughly invested from Brazilian sector by Venkatesh et al. (2017) and Southeast Asian sector by Tulasi Ram et al. (2015). The EEJ becomes sharply negative around 1400 UT due to overshielding electric fields associated with sharp northward turning of IMF *Bz* (Figure 1b). However, the IMF *Bz* quickly returned to southward at ~1410 UT and EEJ also recovered from westward to eastward concurrently. Since then, the

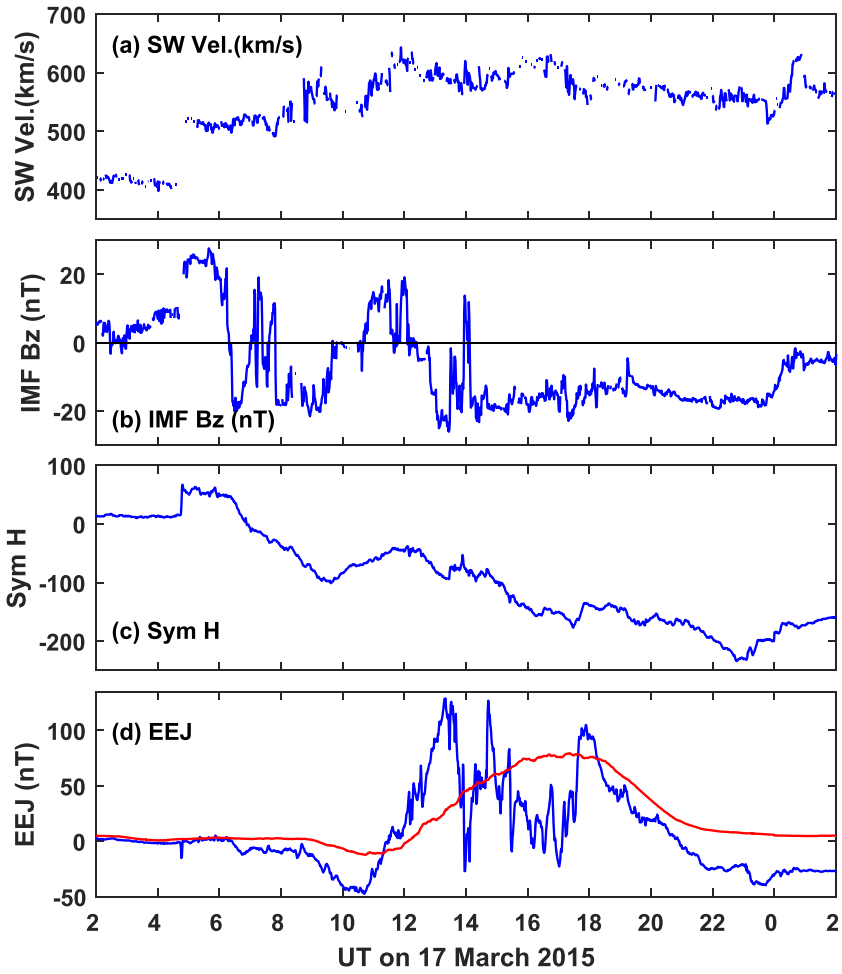

Figure 1. Universal time variations of (a) solar wind velocity, (b) IMF *Bz*, (c) Sym-H index, and (d) equatorial electrojet (EEJ) strength derived from two ground-based magnetometers over Brazil sector during the St. Patrick's Day storm on 17 March 2015. The red curve in (d) represents the mean EEJ variation of five internationally quiet days over Brazil.

IMF *Bz* remained to be steadily southward from 1410 UT for several hours. However, the EEJ strength is mostly less than its quiet day mean values after 1410 UT except the brief excursions around ~1445 and ~1800 UT. The less EEJ values during the noon and afternoon hours over Brazilian sector indicate the prevailing westward DDEFs driven by global-scale wind dynamo action. Huang et al. (2016) and Hairston et al. (2016) have shown the strong DDEF effecting on equatorial and low-latitude ionosphere started from 3–4 hr after the onset of main phase. Tulasi Ram et al. (2015) have shown the strong neutral wind disturbances in the nightside using Fabry-Perot interferometer observations from two conjugate midlatitude stations Shigaraki (Japan) and Darwin (Australia) in Northern and Southern Hemispheres, respectively. They have shown that the meridional neutral wind becomes strongly equatorward and zonal wind turns strongly westward around 1400 UT at both the conjugate northern and southern hemispheric stations indicating the ionospheric disturbance dynamo effects (Figure 5 of Tulasi Ram et al., 2015). Later Zhang et al. (2017) have reported an intense equatorward wind disturbance (>200 m/s) from the Millstone Hill incoherent scatter radar observations in American sector (dayside). The consistent neutral wind disturbances in both dayside and nightside indicate that the disturbance dynamo effects which cause westward DDEF on dayside are prevailing in the background.

Although the IMF *Bz* is steadily southward and the simultaneous westward DDEFs are prevailing in the background, the EEJ strength exhibits several intense and sharp excursions indicating the episodic PPEF events between 1410 and 1900 UT, which are not associated with any significant change in the orientation of IMF *Bz*. In the rest of this paper, we focus our investigation on these intense and sharp PPEF events under

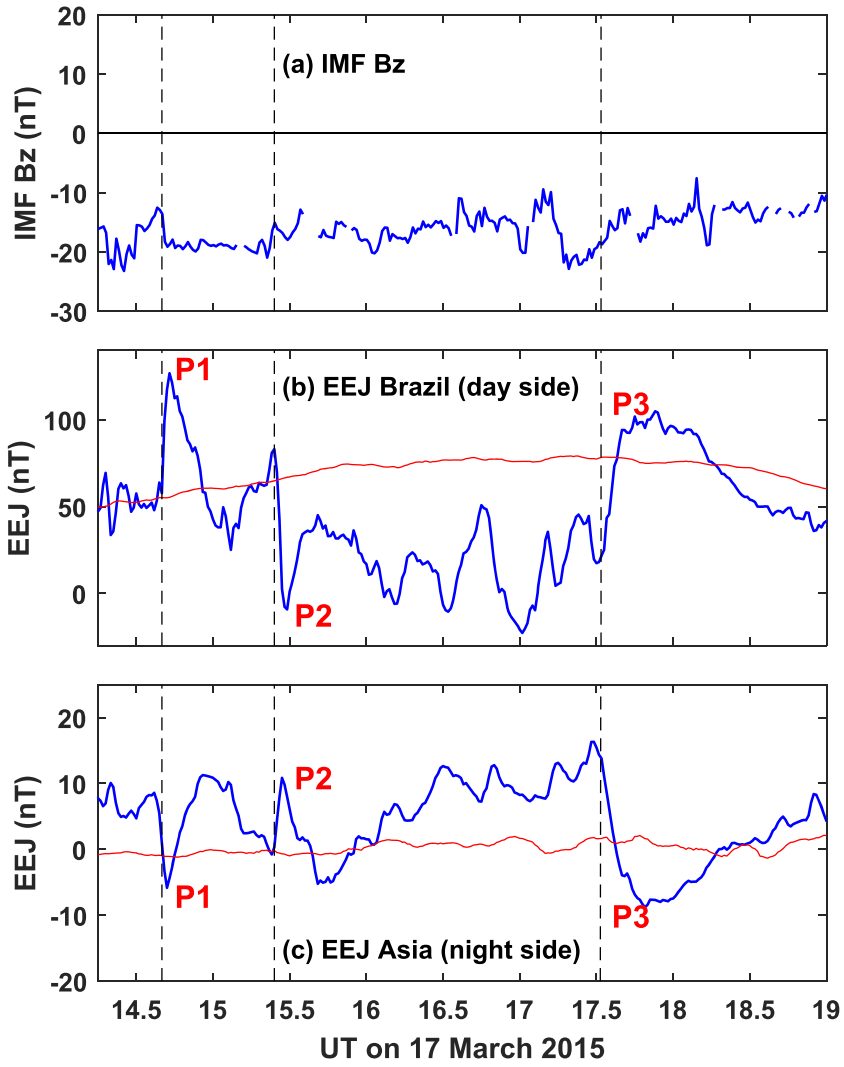

Figure 2. UT variations of IMF *Bz* (a), EEJ variations over Brazil (b), and Asian (c) sectors during the steady southward IMF *Bz* phase between 1425 and 1900 UT on 17 March 2015. The red curves in (b) and (c) represent the mean EEJ variation of five internationally quiet days at the respective locations. The vertical dashed lines represent the UT times of inflections in EEJ during the three penetration events (P1, P2, and P3).

steady IMF *Bz* condition. In order to have a closure look at these PPEF events, the IMF *Bz* and EEJ variations between 1410 and 1900 UT are presented in Figures 2a and 2b, respectively. Further, the EEJ strength from the midnight (2230–0320 LT) sector derived from two ground based magnetometers at Davao and Muntinlupa in the Asian sector is shown in Figure 2c. The red curves in Figures 2b and 2c show the quiet day mean EEJ variations at the respective sectors. The local times over the Belem and Davao (equatorial magnetometer stations in Brazil and Asian sectors) vary from 1100 to 1550 and 2230 to 0320 LT during this period representing the dayside and nightside conditions, respectively. It can be seen from Figure 2a that the IMF *Bz* is steadily southward throughout this period. However, the EEJ in the dayside (Figure 2b) exhibits three sharp and distinct excursions labeled as P1, P2, and P3. The magnitudes of the EEJ excursions at P1, P2, and P3 are 80, −89, and 85 nT, respectively. The universal times at the start of these sharp EEJ inflections are marked as vertical dashed lines at 1440, 1526, and 1732 UT, respectively. The corresponding local times at Belem are 1130, 1216, and 1422 LT, respectively. The EEJ on the nightside (Figure 2c) also exhibits concurrent sharp changes, however, with opposite polarity. It is important to mention here that the ionospheric conductivity in the local midnight sector will be very low to conduct the significant current. Nevertheless, Rastogi et al. (1996) have confirmed that a finite current still can flow in the nighttime equatorial ionosphere. The sharp and concomitant changes with opposite polarities in dayside and nightside

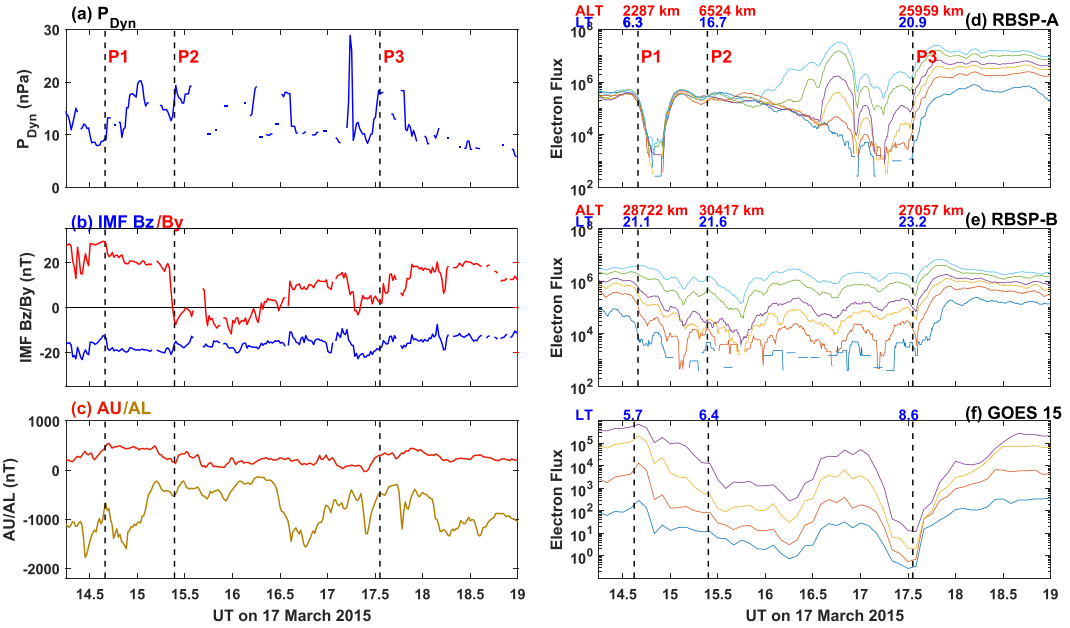

Figure 3. The left panels show the UT variations of (a) solar wind dynamic pressure, P_{Dyn}, (b) IMF *Bz* and *By*, and (c) AU/AL indices. The right panels show the UT variations of kiloelectron volt range electron fluxes measured from (d) RBSP-A, (e) RBSP-B, and (f) the geosynchronous GOES-15 satellites during the steady southward IMF *Bz* phase between 1425 and 1900 UT. The vertical dashed lines represent the UT times of inflections in EEJ during the three penetration events (P1, P2, and P3). The local times and orbital altitudes of RBSP-A and B are indicated on top of the respective panels. Please refer text for more details.

further reassure that the observed changes (at P1, P2, and P3) are due to disturbances in the ionospheric electric field caused by PPEF. However, the magnitudes of the observed changes in the nightside equatorial current are significantly smaller compared to the dayside (note the *Y* axis scale difference between Figures 2b and 2c) due to very low conductivity in the nightside. The EEJ in dayside (Figure 2b) exhibits other relatively small fluctuations between 1530 and 1730 UT. However, these fluctuations are rather gradual and the signatures with opposite polarity were not clearly observed in the nightside (Figure 2b). Hence, they are debatable to be called as penetration events, and thus, not studied further in this paper (although worth to be investigated in future).

In order to investigate the factors responsible for the three PPEF events (P1, P2, and P3), the solar wind parameters and substorm activity are examined. The left-hand side panels of Figure 3 show the temporal variations of solar wind dynamic pressure (P_{Dyn}, Figure 3a), dawn-to-dusk, and vertical components of IMF (*By* and *Bz*, Figure 3b), and the eastward and westward auroral electrojet indices (AU/AL, Figure 3c). The three vertical black dashed lines in all panels of Figure 3 represent the UT of Penetration Events P1, P2, and P3. The observation of AU/AL indices in Figure 3c indicates an enhanced auroral activity (decrease in AL) during P1; and short-lived decreases in AL few minutes before and after P3. However, no significant decrease in AL is observed around P2. It is known that the large fluxes of energetic particles (both electrons and protons) will be injected into the magnetosphere, particularly, in the nightside during the onset of substorm expansion phase. The particle injections can be detectable as a dispersion less enhancement of in situ particle fluxes measured from the satellites in the inner magnetosphere (e.g., Reeves et al., 2003). Therefore, in order to examine the presence or absence of substorm activity during the above PPEF events (P1, P2, and P3), the energetic (~75- to 500-keV range) electron flux injections from RBSP-A, RBSP-B, and GOES-15 satellites are presented in Figures 3d–3f, respectively. The RBSP-A and -B are twin satellites in 10° inclination elliptical orbit with perigee of 605 and 625 km and apogee of 30,410 and 30,540 km, respectively. The local times and orbital altitudes of RBSP-A and -B corresponding to the P1, P2, and P3 are indicated on the top of Figures 3d and 3e. The GOES-15 is a geosynchronous satellite at 135°W longitude, and the corresponding local times at P1, P2, and P3 are indicated on top of Figure 3f. During the P1 and P2, the RBSP-A is near its perigee and rapidly progressing from dawn to afternoon (Figure 3d) sectors. Note that the rapid

decrease and increase in the electron flux between 1430 and 1500 UT from RBSP-A (Figure 3d) is due to the progression of space craft through ionosphere (out of radiation belts) near its perigee. The RBSP-B (Figure 3e) is in the nightside (~21 LT) at 28,722-km altitude and the geosynchronous GOES-15 (Figure 3f) is at the dawnside during P1 and P2. The electron fluxes observed from both the RBSP-B (nightside) and GOES-15 (dawnside) did not exhibit any clear signature of particle injection due to the onset of substorm during P1 and P2. During P3, the RBSP-A and B are in the nightside (2048 and 2312 LT, respectively) and GOES-15 is in the morning (0830 LT) sector. It can be seen from Figures 3d–3f that the electron fluxes from all three satellites exhibit a rapid increase indicating the injection of energetic particles, probably, due to the onset of a substorm expansion at P3.

A careful examination of the solar wind parameters in Figures 3a and 3b reveals that the P1 event is associated with a small but simultaneous increase in P_{Dyn} and decrease in IMF *Bz* (and *By*). The P_{Dyn} is increased from ~8 to 13 nPa)Figure 3a), and IMF *Bz* is decreased from −13.6 to −18.3 nT (become more southward) (Figure 3b). Although it is a small increase in P_{Dyn}, the simultaneous decrease in the IMF *Bz* might have caused the eastward PPEF in the dayside and sharp increase of EEJ by about 80 nT at 1440 UT (Figure 2b). Although the AL index exhibits a significant decrease during P1 (Figure 3c), it may not be associated with a substorm as the particle injections were not observed in the nightside from the RBSP-B (Figure 3e). Nevertheless, the increase in EEJ at P1 (Figure 2b) is quite rapid compared to the rate of decrease in AL (Figure 3c). Hence, it is unlikely that the sharp eastward PPEF at P1 is effected by the substorm, if any. The decrease in AL during P1 could be due to enhanced convection current in the polar region due to the simultaneous decrease of *Bz* and increase of $P_{Dyn.}$

The increase in the low-latitude ionospheric electric field due to increase in the solar wind pressure during the arrival of interplanetary shocks has been earlier reported by Huang et al. (2008) and Zong et al. (2010). Later, Wei et al. (2012) have shown that the solar wind pressure (mainly solar wind density) controls the convection electric field under polar cap saturation conditions and causes PPEF during the main phase of a superstorm on 20 November 2003. Most of the previous reports on solar wind pressure induced PPEF are either during the arrival of intense interplanetary shocks (Huang et al., 2008; Zong et al., 2010) or during the period of polar cap saturation under dominant background convection electric fields (Wei et al., 2012). However, the uniqueness of the present case (P1) is that it occurred at the later part of the main phase where the DDEFs are prevailing in the background as discussed earlier. In other words, the PPEF during the P1 has overcome the background DDEF and caused large enhancement of eastward EEJ current in the dayside ionosphere (and westward current on the nightside).

The second PPEF event (P2) that caused a sharp negative excursion of EEJ by 89 nT at 1526 UT does not appear to be associated any significant change in IMF *Bz* (Figure 2b). However, the dawn-to-dusk component of IMF that is, IMF *By* turned sharply from duskward to dawnward (from 19.5 to −7.6 nT). Interestingly, a small increase in P_{Dyn} (~6 nPa) can also be noticed from Figure 3a at the same time. The increase in the P_{Dyn} is expected to cause an eastward PPEF in the dayside ionosphere according to previous reports by Huang et al. (2008), Zong et al. (2010) and Wei et al. (2012) as well as the PPEF event P1 presented earlier. However, the P2 exhibited a westward (eastward) electric field disturbance in the dayside (nightside) ionosphere, that is, opposite to the expected PPEF effect due solar wind pressure increase. Therefore, the negative EEJ excursion at P2 can be attributed to the sharp reversal of IMF *By*. Observations of PPEFs at equatorial ionosphere due to changes in IMF *By* are very sparse. Kelley and Makela (2002) have reported an eastward pulse of equatorial zonal electric field at Jicamarca around postsunset hours corresponding to southward turning of IMF *Bz*. They have considered it as an opposite polarity compared to the expected PPEF due to southward turning of IMF *Bz* and attributed to the effect of positive IMF *By*. Recently, Chakrabarty et al. (2017) have shown a clear example of westward (eastward) PPEF in the dayside (nightside) due to sharp dawnward to duskward (negative to positive) turning of *By* under steady southward *Bz*. They have also observed the eastward electric field perturbations simultaneously on both dayside and nightside when the *By* is turned from duskward to dawnward (positive to negative). In contrast, the present P2 event is an impeccable example of westward (eastward) PPEF in the dayside (nightside) ionosphere associated with a sharp reversal in IMF *By* from positive to negative barring any significant change in the *Bz*.

The third PPEF Event P3 caused a strong enhancement in the dayside EEJ (by ~85 nT) despite the prevailing background westward EEJ (Figure 3e). This P3 event is coincided with a solar wind dynamic pressure

increase of the order of ~8 nPa, which is expected to contribute to the eastward PPEF in the dayside (Huang et al., 2008; Sibeck et al., 1998; Wei et al., 2012; Zong et al., 2010) similar to that observed at P1. Further, the short-lived decreases in AL few minutes before and after the P3 (Figure 3c); and the dispersion less increase in the kiloelectron volt electron fluxes from RBSP-A, RBSP-B, and GOES-15 (Figures 3d–3f) indicate the possible onset of a substorm around P3. Recently, Venkatesh et al. (2019) have shown the large and sudden increase in Wp index at the same time (1730 UT) as P3 (Figure 2e of Venkatesh et al., 2019). The Wp index is computed from the wave power of Pi2 pulsations from about 11 low-latitude geomagnetic field observations (Nosé et al., 2009). A sharp increase in Wp index along with the dispersionless injection of energetic electron fluxes at geosynchronous altitudes are found to be good indicators for the onset of substorms (e.g., Nosé et al., 2009, 2012; Reeves et al., 2003). Therefore, in view of the signatures observed in PDyn (Figure 3a), AL (Figure 3c), kiloelectron volt electron fluxes measured in the inner magnetosphere (Figures 3d–f), and Wp index (Figure 2d of Venkatesh et al., 2019), we attribute the strong and sustained (about 45 min) enhancement in EEJ at P3 to the solar wind dynamic pressure pulse followed by the onset of a substorm under steady southward IMF *Bz* conditions.

3.2. Effect on EIA

This section presents the effects of the PPEF events on the EIA over Brazilian longitudes. In Figure 4, we show the ionospheric TEC variations as a function of UT and geomagnetic latitude over Brazilian sector obtained from the madrigal database in comparison with EEJ variations. The madrigal GPS-TEC map data consist of vertical TEC measurements from worldwide distributed GPS receivers binned in 1° latitude by 1° longitude (Geographic) grid at 5-min intervals (Rudeout & Coster, 2006). The corresponding geomagnetic latitudes for each data point have been computed using the IGRF-2012 model (Thébault et al., 2015). The vertical TEC data over a narrow Brazilian longitude sector (50–60°W) on 17 March 2015 were selected and plotted as a function of UT and geomagnetic latitude in Figure 4b. The TEC on a previous quiet day (15 March 2015) is also shown for reference in the bottom panel. A strong positive ionospheric storm can be observed on 17 March (Figure 4b) compared to previously quiet day (Figure 4c). The Penetration Events P1 and P2 did not appear to cause any significant changes in the TEC distribution, perhaps, due to the brevity of the electric field disturbances. Interestingly, the latitudinal distribution of TEC is highly asymmetric during the period between P2 and P3 (Figure 4b). The TEC in the southern low latitudes becomes nearly double that of quiet day while the TEC in the northern low latitudes (~0°N to 20°N) is slightly smaller compared to the quiet day TEC. Further, this asymmetric positive (negative) TEC storm at southern (northern) low latitudes between P2 and P3 occurred during the period when the EEJ is significantly smaller compared to its quiet day mean curve (Figure 4a). This suggests that the observed asymmetric TEC storm occurred during the period when the westward DDEFs are prevailing in the background. During the same period, a strong equatorward (100–250 m/s) and westward (200–300 m/s) neutral wind surge has been observed in both the hemispheres from two Fabry-Perot interferometers in Japan-Australian (local midnight) sector by Tulasi Ram et al. (2015). Zhang et al. (2017) have also reported a large equatorward wind (>200 m/s) in the American sector (dayside) during the same period. The strong equatorward and westward neutral wind surge consistently observed in the dayside and nightside indicate that the observed hemispheric asymmetry in the TEC on 17 March (Figure 4b) is mainly due to the neutral wind dynamo-driven disturbances. In the absence or weakening of upward E × B drift (and equatorial fountain) due to westward DDEF, the plasma distribution at low latitudes will be dominantly altered by the neutral winds. The equatorward wind causes field-aligned upward transport of plasma to the higher altitudes where the recombination loss is small. Further, the declination angles of field lines are largely westward in the Brazilian sector. Titheridge (1995) has given the relationship for the effective upward/downward field-aligned transport of plasma in the ionosphere as

$$V_{up} = \left(W_{equ} \cos D \pm W_{east} \sin D\right) \cos I \sin I \quad (1)$$

Here, W_{equ} is meridional wind (equatorward positive), W_{east} is zonal wind (eastward positive), and + and − signs apply in the Southern and Northern Hemispheres, respectively. Therefore, the equatorward and westward neutral wind surge becomes more effective in upward transport of plasma in the southern magnetic low latitudes leading to strong positive ionospheric storm in the Southern Hemisphere. On the other hand, westward neutral wind causes a downward plasma transport due to westward (negative) declination angle of field lines in the Brazilian sector leading to higher recombination loss of plasma in northern low latitudes.

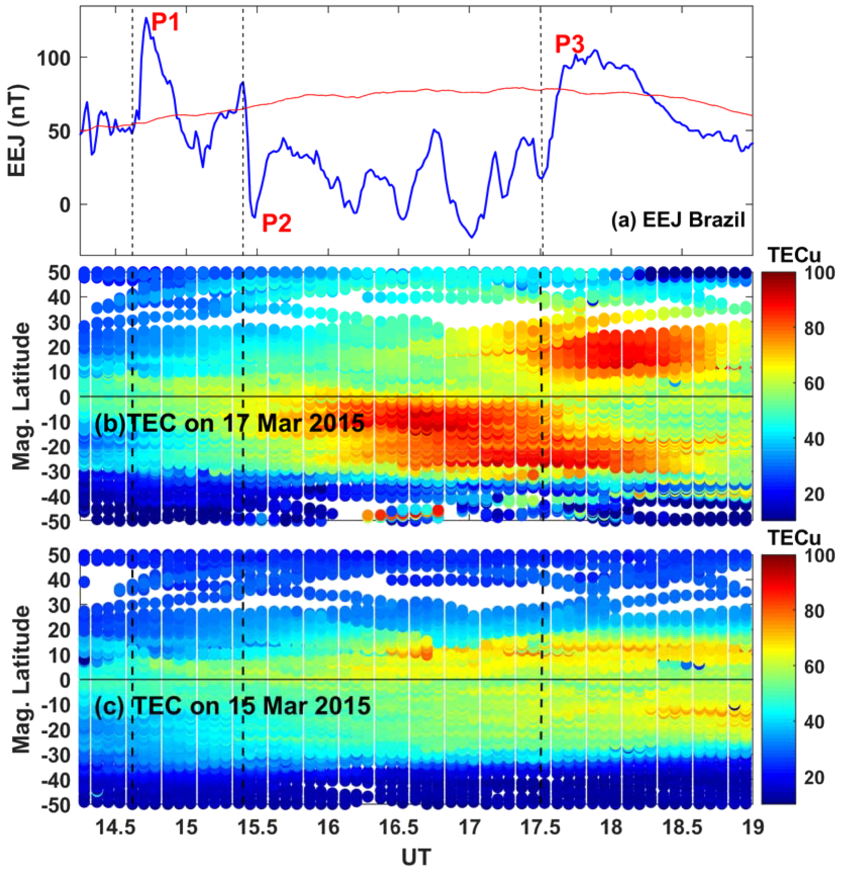

Figure 4. (a) The EEJ variation over Brazil. (b) The geomagnetic latitudinal and UT variation of ionospheric total electron content (TEC) from Brazilian sector on 17 March 2015. (c) The TEC distribution on the previously quiet day (15 March 2015) for comparison.

Further, the nondipolar nature of the geomagnetic field, that is, the large offset between the geographic and geomagnetic equators, also positively contributes to the observed hemispheric asymmetry in TEC over this sector.

Another interesting observation in Figure 4b is the rapid (almost sudden) latitudinal redistribution of TEC with the PPEF at P3. The equatorial plasma quickly redistributed to the low latitudes forming a nearly symmetric EIA during P3. For example, Figure 5 shows the geomagnetic latitudinal variations of TEC from 1700 to 1815 UT at 15-min interval. The vertical lines in the subpanels indicate the geomagnetic equator. It can be seen from these panels that the latitudinal distribution of TEC is asymmetric with larger values in the southern magnetic latitudes and southern EIA crest located much closer to the equator during 1700 and 1715 UT. At 1730, the TEC at equatorial latitudes started depleting via equatorial fountain process (Balan & Bailey, 1995) due to the eastward PPEF at P3. This can be observed as decrease of TEC close to the equator, poleward movement of southern EIA crest, and strengthening of northern EIA crest. The plasma is quickly redistributed and the EIA with clear trough at the equator and nearly symmetric crests in northern and southern low latitudes are formed by 1745 UT. This quick redistribution of plasma (within 15 min) and formation of symmetric EIA indicates the domination of strong equatorial fountain process, often known as super plasma fountain due to strong eastward PPEF (Balan et al., 2009; Mannucci et al., 2005), over the background neutral wind-driven asymmetric plasma transport happened between P2 and P3. In other words, the field-perpendicular plasma transport via E × B drift due to strong eastward PPEF is dominated over the field-aligned plasma transport by prevailing disturbance neutral winds over equatorial and low latitudes. This quick and symmetric development of EIA (Figure 5) is the most convincing evidence for the strong eastward PPEF and a possible equatorial super fountain effect due to solar wind pressure pulse followed by the onset of substorm under steady southward IMF *Bz*.

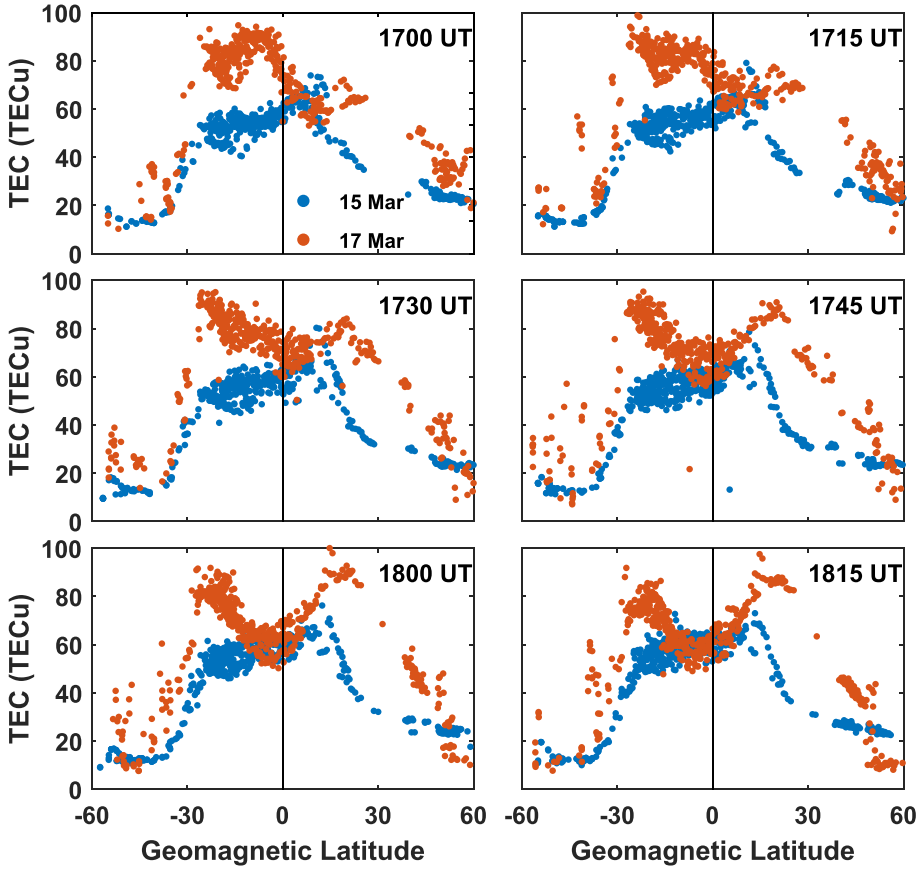

Figure 5. Geomagnetic latitudinal distribution of TEC over Brazilian sector from 1700 to 1815 UT at 15-min intervals on 17 March (red filled circles) in response to the PPEF event due to the substorm. The blue filled circles represent the TEC on previously quiet day (15 March) for comparison.

4. Discussion

It is widely known that the southward or northward turnings of IMF *Bz* cause prompt penetration of undershielding or overshielding electric fields to low-latitude ionosphere. In the previous section, we have presented the three sharp PPEF events occurred under steady southward IMF *Bz* period without any significant changes in the orientation of IMF *Bz*. Further, these events have occurred nearly 8 hr after the onset of main phase and during the period when the strong DDEF effects are prevailing in the background. The first PPEF event (P1) occurred at 1440 UT caused a sharp increase in the dayside EEJ strength by ~80 nT over Brazilian sector with a concomitant negative excursion in the nightside. Although there is no prominent southward excursion of *Bz*, a marginal but simultaneous decrease in *Bz* of the order of 5 nT (Figure 3b) and a simultaneous increase in pressure (P_{Dyn}) by ~5 nPa (from ~8 to ~13 nPa) (Figure 3a) have caused an eastward PPEF and a sharp increase (decrease) in EEJ in dayside (nightside). The solar wind velocity is increased from ~583 to 596 km/s and density is increased from ~16 to 22 particles per cubic centimeter (not shown in the figure) suggesting this pressure pulse is mainly due to the increase in solar wind density. The enhanced equatorial current and short-lived electric field perturbations during the preliminary impulse of storm sudden commencement due to increased pressure have been earlier detected from ground based magnetometers (Kikuchi et al., 2001; Kikuchi & Araki, 1985) and HF Doppler observations (Sastri et al., 1993). Later, Huang et al. (2008) and Zong et al. (2010) have shown the increase in dayside ionospheric eastward electric field due to increase in the P_{Dyn} during the arrival of interplanetary shocks using Jicamarca incoherent scatter radar and Digisonde observations, respectively. Huang et al. (2008) have also observed an increase in high-latitude convection electric field associated with Region-1 field-aligned currents during the solar wind pressure enhancement and attributed that the observed enhanced low-latitude ionospheric electric field is due to prompt penetration of polar ionospheric dawn-to-dusk electric field. Wei et al.

(2012) have also shown that the solar wind pressure (mainly solar wind density) controls the convection electric field under polar cap saturation conditions and causes PPEF during the main phase of a superstorm on 20 November 2003. Therefore, the observed eastward PPEF (enhanced EEJ) at P1 in Figure 2b is consistent with the PPEF effects due to the solar wind pressure enhancements reported in the earlier studies. However, most of the previous reports on solar wind pressure induced PPEF are either during the arrival of intense interplanetary shocks (Huang et al., 2008; Zong et al., 2010) or during the period of polar cap saturation under dominant background convection electric fields (Wei et al., 2012). On the other hand, present case (P1) occurred during the phase when the DDEFs are prevailing in the background. This indicates that the PPEF during the P1 has overcome the background DDEF and caused large enhancement of eastward (westward) current in the dayside (nightside) ionosphere. Recently, Rout et al. (2016) have shown the eastward PPEF over Indian sector around the similar local times (~1030 LT) due to solar wind density enhancement under steady northward IMF *Bz*. However, the observed change in EEJ strength is very weak (only ~3–4 nT) in their case (Figure 5f of Rout et al., 2016). The very small increase in EEJ in Rout et al. (2016) could be probably due to increase in solar wind density alone under steady northward IMF *Bz*. Therefore, the comparison of EEJ enhancement at P1 with that of Rout et al. (2016) around similar local times suggests that the decrease in IMF *Bz* simultaneously with the pressure pulse could have played a key role in the strong eastward PPEF causing the large enhancement in EEJ during P1.

The second PPEF event (P2) occurred at 1526 UT have caused a sharp decrease in EEJ (counter electrojet) by about 89 nT (westward PPEF) in the dayside (Figure 2b). This westward PPEF event at P2 is not associated with any significant change in IMF *Bz*, however, with a sharp turning of IMF *By* from duskward to dawnward (+ve to −ve) (Figure 3b). A small increase in P_{Dyn} also observed at the same time; however, it does not appear to have much effect as the observed change in EEJ is negative during P2 in contrast to the expected increase in EEJ due to pressure pulse as discussed before. The role of IMF *By* on the prompt ionospheric electric field disturbance in both dayside and nightside has been recently reported by Chakrabarty et al. (2017). They have shown that a sharp dawnward to duskward (−ve to +ve) turning of *By* has caused westward (eastward) PPEF over Jicamarca (Thumba) in the dayside (nightside) ionosphere under steady southward IMF *Bz*. The observed westward (eastward) PPEF in the dayside (nightside) is attributed to the clockwise rotation of high-latitude convection cells and the electrodynamic divider between the dawn and dusk cells. It is explained by Chakrabarty et al. (2017) that due to this clockwise rotation of the electrodynamic divider associated with dawnward to duskward turning of *By*, the Jicamarca (dayside observation) came under dusk cell and Thumba (nightside observation) is encompassed by dawn cell causing the westward and eastward PPEFs in dayside and nightside, respectively. The clockwise and counterclockwise rotations of high-latitude convection cells due to respective duskward and dawnward turnings of *By* have also been reported earlier by Heelis (1984), Ruohoniemi and Greenwald (2005), and Tanaka (2007). Thus, a counterclockwise rotation of high-latitude convection cells is expected due to duskward (+ve) to dawnward (−ve) turning of *By* in the case of P2. The local time over Brazil during P2 is ~1210 LT, that is, just only a few minutes into the postnoon sector. Hence, the expected counterclockwise rotation of high-latitude convection cells (or electrodynamic divider) causes the dawn cell to rotate toward noon meridian, that is, closer toward noon and possibly encompass the Brazil sector. This would expect to cause an eastward PPEF (increase in EEJ). However, the exactly opposite (decrease in EEJ) is observed at P2. The ionospheric convection maps constructed from SuperDARN observations have been examined for the possible rotation of high-latitude convection cells. However, no significant rotation of convection cells has been observed during this period. For the reference of reader, the SuperDARN convection maps from Northern and Southern Hemispheres during 1520 to 1530 at 2-min intervals are provided in the supporting information (Figures S1a and S1b). It is important to mention here that the SuperDARN maps during this period contain very less observations (velocity vectors), hence, considered only for a reference with caution.

Penetration of convection or overshielding electric fields to low latitudes is mainly known to occur due to the imbalance between the Region-1 and Region-2 field-aligned currents in the high-latitude ionosphere (Kikuchi et al., 2000, 2003). Iijima and Potemra (1976) have identified an additional Birkeland current system poleward of Region-1 system between 0930 and 1430 MLT, known as polar cusp current system. The flow direction of this additional current system is opposite to that of Region-1 currents, that is, flows away from (into) the ionosphere in the dawnside (duskside) ionosphere. Thus, the high-latitude electric field potential depends on the net field-aligned current distribution in the midday cusp region (0930–1430

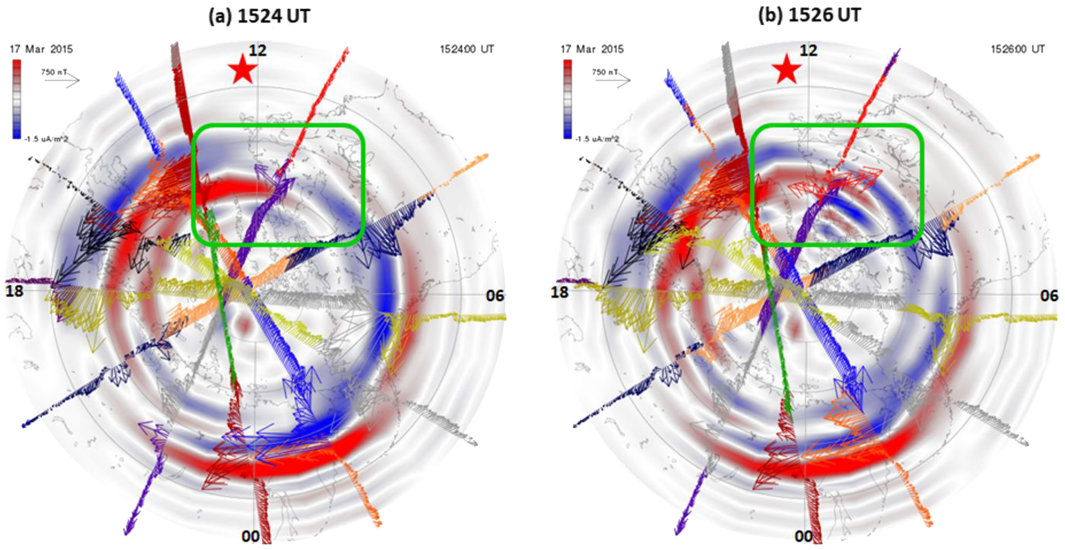

Figure 6. (a, b) The reduced horizonal magnetic field perturbations (vectors) from the AMPERE and the derived radial currents (filled contours in red and blue colors) using curl of spherical harmonic fit of magnetic field perturbations. The red star indicate the MLT location of the Belem (the equatorial magnetometer station in Brazil) (refer text for more details).

MLT) and the Region-1 current system dominates outside this region (Iijima & Potemra, 1976). Further, Iijima et al. (1978) and Erlandson et al. (1988) have shown that the direction of this polar cusp current system strongly depends on the direction of IMF *By*. They have observed that duskside field-aligned Birkeland current that flows into the ionosphere extends to the prenoon sector when IMF *By* is negative and the dawnside current that flows away from the ionosphere extends to postnoon sector when IMF *By* is positive.

In order to examine the possible changes in the high-latitude field-aligned (Birkeland) currents during P2, the reduced horizontal magnetic field residuals and the derived radial currents from the Active Magnetosphere and Planetary Electrodynamics Response Experiment (AMPERE) using the constellation of Iridium satellites have been considered. The arrows in Figure 6 represent the magnetic field (H) perturbations measured from different Iridium satellites (different colors) using a reference arrow on the left top corners. The filled contours in blue and red colors indicate the radial currents into (−ve, blue) and away from (+ve, red) the ionosphere derived from the curl of spherical harmonic fit to the magnetic perturbations. Figures 6a and 6b correspond to 1524 and 1526 UT, respectively. The red star in Figures 6a and 6b indicates the MLT sector of the Belem (the equatorial magnetometer in Brazil) at the respective times. The Region-1 and Region-2 field-aligned currents can be clearly observed from these figures. One interesting observation that can be noted from Figure 6b is that the disruption/weakening of Region-1 currents and development of additional current system (cusp current) on the poleward of Region-1 around noon MLT sector at 1526 UT (as marked by green rectangle). This is the time correspond to the negative inflection in the EEJ (P2) associated with duskward to dawnward reversal of IMF *By*. It should be noted that the IMF *Bz* is steadily southward for about 1 hr before P2. Thus, it is expected that the convection electric field due to Region-1 current and the shielding electric fields due to Region-2 currents are more or less stable and the net electric field had been established. Under this stable situation of Region-1 and Region-2 current systems, the sharp dawnward turning of *By* could have caused the enhanced polar cusp currents in the noon MLT sector, which is opposite to the Region-1 currents as observed in Figure 6b. This could result in the net decrease of convection electric field due to the Region-1 currents. Due to this net decrease in Region-1 field-aligned currents, the shielding electric fields associated with Region-2 currents would momentarily dominate over the convection electric fields and can result in a westward PPEF (counter electrojet) as observed during P2. However, it is important to mention here that the above mechanism is one possible explanation for the observed westward PPEF during P2 and needs to be entrenched with statistically significant number of observations.

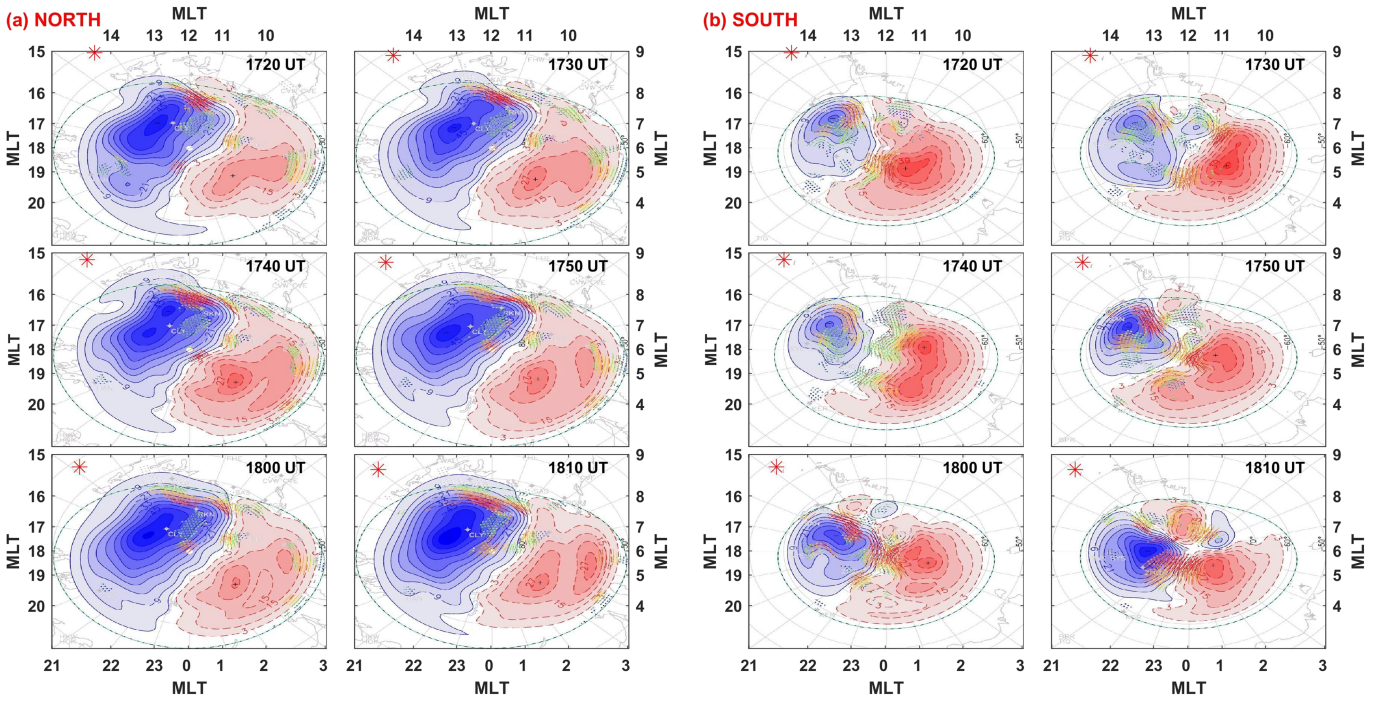

Figure 7. High-latitude convection maps constructed from SuperDARN HF radars in (a) Northern and (b) Southern Hemisphere during 1720 to 1810 at 10-min intervals. The red asterisk (*) in each panel represents the MLT of equatorial magnetometer station (Belem) used in this study.

The third penetration event (P3) is associated with the solar wind dynamic pressure pulse followed by a substorm and has caused a strong enhancement in EEJ (by ~85 nT) in the dayside even under the prevailing westward DDEFs in the background (Figure 2b). With a view to understand the possible mechanisms for the observed eastward PPEF at P3, the high-latitude convection maps from the SuperDARN HF radars have been examined. Figures 7a and 7b present the SuperDARN convection maps at Northern and Southern Hemispheres, respectively, from 1720 to 1810 UT at 10-min intervals. The red asterisk in each panel indicates the MLT sector of Belem at respective times. The Belem is located in the afternoon MLT sector (~1420 to 1500 LT) during the period of substorm onset and expansion (~1730–1810 UT). It can be seen from this figure that the high-latitude convection field does not appear to alter much in the Northern Hemisphere (Figure 7a) during 1730 to 1810 UT. It should be noted again here that the velocity vectors from SuperDARN HF radar observations, particularly, in the nightside MLT region are very less during this period in the Northern Hemisphere. Hence, the constructed convection maps are mostly based on the convection model in the Northern Hemisphere. However, the convection field in the Southern Hemisphere (Figure 7b) exhibits a significant distortion and/or reconfiguration. The reconfiguration of convection maps can be observed starting from 1730 UT, particularly, at the noon MLT sector where the sufficiently large number of observations (see the vectors) is available. As the time progresses, the dawn cell expands (dusk cell shrinks) during 1740 to 1750 UT, and two small cells with opposite polarity to that of primary cells formed by 1800 UT, which further strengthened at 1810 UT. This reconfiguration of convection cells in the southern high latitudes indicates the modification of high-latitude field-aligned current system and the resultant convection electric field. From Figure 7b, it can be noticed that Belem happens to be located between the newly formed positive cell in the noon sector and the primary negative cell in the dusk sector. Hence, it experiences an additional eastward electric field perturbation due to the newly formed convection cells in addition to the primary dawn-to-dusk convection electric field in the dayside. Therefore, the observed strong enhancement in EEJ at P3 in the Brazil sector (Figure 2b) can be attributed to the eastward PPEF owing to the reconfiguration of high-latitude convection cells in the Southern Hemisphere. The induced eastward electric field perturbation during P3 is significantly large that caused strong equatorial fountain effect and quick redistribution of EIA over the Brazilian sector as discussed before (Figures 4 and 5).

5. Summary and Conclusions

In this paper, we presented three episodes of PPEF with opposite polarities on dayside and nightside during the main phase of St. Patrick's Day storm on 17 March 2015 without involvement of changes in the direction of IMF *Bz*. Further, these events have occurred during the period when the strong DDEF disturbances are prevailing in the background. The first event is caused by increase in the solar wind dynamic pressure by ~5 nPa that led to eastward PPEF and a sharp increase of EEJ by ~89 nT in the Brazilian sector (dayside). This event is also coincided with the decrease of southward IMF *Bz* (become more southward) by ~5 nT. Therefore, the large increase in the EEJ is attributed as due to the combined action of solar wind pressure pulse and simultaneous decrease in IMF *Bz* during this first episode. The second PPEF event caused sharp decrease in EEJ (westward PPEF) by ~85 nT associated with the sharp dawnward to duskward turning of IMF *By* under steady southward IMF *Bz*. The high-latitude convection maps constructed from the SuperDARN HF radar network observations indicate that there is no significant rotation of convection cells during this episode in both hemispheres. On the other hand, the reduced magnetic field (H) perturbations from the AMPERE indicate the disruption/weakening of Region-1 currents and development of enhanced polar cusp current during P2. Hence, we speculate that the observed westward PPEF could be associated with the enhanced polar cusp currents around noon sector and the resultant decrease of net convection electric fields at high latitudes due to sharp duskward to dawnward turning of *By* (Erlandson et al., 1988; Iijima et al., 1978; Iijima & Potemra, 1976). The third PPEF event is coincided with a solar wind dynamic pressure pulse followed by a substorm and has caused large increase in EEJ on the dayside that lasted for relatively long period. The strong eastward PPEF during this event has caused the equatorial super fountain (Balan et al., 2009) and rapid redistribution of low-latitude plasma into symmetric EIA crests within 15 min (Figures 4 and 5) over the Brazilian sector. The high-latitude convection maps from SuperDARN observations indicate that the reconfiguration of convection cells in the southern high latitudes during P3 and the resultant enhancement of convection electric field led to this eastward (westward) PPEF on dayside (nightside). The PPEF events presented in this paper are different from the conventional PPEFs associated with the changes in the IMF *Bz* orientation and gives better understanding on the equatorial and low-latitude ionospheric and geomagnetic field disturbances associated with PPEFs.

Acknowledgments

This work is partly supported by Department of Science and Technology, Government of India and ISEE, Nagoya University, under international joint research program 2019. This research was also supported by the National Key R&D Program of China (2018YFC1407304, 2018YFC1407303), the National Natural Science Foundation of China (41604139, 41574138, 41774166, 41431072, 41831072), and the Foundation of National Key Laboratory of Electromagnetic Environment (grants 6142403180103, 6142403180102). The work of K. Shiokawa is supported by JSPS KAKENHI (15H05815 and 16H06286). One of the authors (K. V.) wishes to express his sincere thanks to NARL, India, for providing fellowship. The authors acknowledge the C. M. Denardini, INPE, Brazil, for providing magnetometer data over Eusebio; E. Yizengaw, E. Zesta, M. B. Moldwin, and the rest of the AMBER and SAMBA team for the magnetometer data over Belem being operated by Boston College and funded by NASA and AFOSR. The magnetometers at Davao and Muntinlupa are operated under MAGDAS network (http://www.serc.kyushu-u.ac.jp/magdas/MAGDAS_Project.htm). The open data policy of Space Physics Data Facility (SPDF), NASA, USA (http://omniweb.gsfc.nasa.gov/ow_min.html) for the solar wind parameters, IMF *Bz*, Sym-H, AU, and AL indices; CDAWeb (http://cdaweb.gsfc.nasa.gov/istp_public/) for the energetic electron fluxes data from GOES-15 at geosynchronous orbit is duly acknowledged. The madrigal TEC data is downloaded from the website (http://madrigal.haystack.mit.edu/cgi-bin/madrigal/madInvent.cgi). The GPS-TEC data products and access through the Madrigal distributed data system are provided to the community by the Massachusetts Institute of Technology under support from U.S. National Science Foundation Grant AGS-1242204. The AMPERE data are obtained from the http://ampere.jhuapl.edu/index.html website, and the SuperDARN data are obtained from the website (http://vt.superdarn.org/tiki-index.php?page=DaViT+Map+Potential+Plot). The kiloelectron volt range electron fluxes from Van Allen Probes-A and B were taken from the https://www.rbsp-ect.lanl.gov/rbsp_ect.php website, and GOES-15 data were obtained from CDAWeb (https://cdaweb.gsfc.nasa.gov/cgi-bin/eval1.cgi).

References

Anderson, D., Anghel, A., Yumoto, K., Ishitsuka, M., & Kudeki, E. (2002). Estimating daytime vertical E × B drift velocities in the equatorial *F* region using ground-based magnetometer observations. *Geophysical Research Letters*, *29*(12), 1596. https://doi.org/10.1029/2001GL014562

Astafyeva, E., Zakharenkova, I., & Förster, M. (2015). Ionospheric response to the 2015 St. Patrick's Day storm: A global multi-instrumental overview. *Journal of Geophysical Research: Space Physics*, *120*, 9023–9037. https://doi.org/10.1002/2015JA021629

Balan, N., & Bailey, G. J. (1995). Equatorial plasma fountain and its effects—Possibility of an additional layer. *Journal of Geophysical Research*, *100*, 21421.

Balan, N., Shiokawa, K., Otsuka, Y., Watanabe, S., & Bailey, G. J. (2009). Super plasma fountain and equatorial ionization anomaly. *Journal of Geophysical Research*, *114*, A03311. https://doi.org/10.1029/2008JA013768

Batista, I. S., Candido, C. M. N., Souza, J. R., Abdu, M. A., de Araujo, R. C., Resende, L. C. A., & Santos, A. M. (2017). *F*3 layer development during quiet and disturbed periods as observed at conjugate locations in Brazil: The role of the meridional wind. *Journal of Geophysical Research: Space Physics*, *122*, 2361–2373. https://doi.org/10.1002/2016JA023724

Blanc, M., & Richmond, A. D. (1980). The ionospheric disturbance dynamo. *Journal of Geophysical Research*, *85*, 1669–1688.

Chakrabarty, D., Hui, D., Rout, D., Sekar, R., Bhattacharyya, A., Reeves, G. D., & Ruohoniemi, J. M. (2017). Role of IMF *By* in the prompt electric field disturbances over equatorial ionosphere during a space weather event. *Journal of Geophysical Research: Space Physics*, *122*, 2574–2588. https://doi.org/10.1002/2016JA022781

Erlandson, R. E., Zanetti, L. J., Potemra, T. A., Bythrow, P. F., & Lundin, R. (1988). IMF *By* dependence of Region 1 Birkeland currents near noon. *Journal of Geophysical Research*, *93*(A9), 9804–9814.

Fejer, B. G., & Scherliess, L. (1997). Empirical models of storm time equatorial zonal electric fields. *Journal of Geophysical Research*, *102*, 24,047–24,056.

Gonzales, C. A., Kelley, M. C., Fejer, B. G., Vickrey, J. F., & Woodman, R. F. (1979). Equatorial electric fields during magnetically disturbed conditions: 2. Implications of simultaneous auroral and equatorial measurements. *Journal of Geophysical Research*, *84*(A10), 5803–5812. https://doi.org/10.1029/JA084iA10p05803

Hairston, M., Coley, W. R., & Stoneback, R. (2016). Responses in the polar and equatorial ionosphere to the March 2015 St. Patrick Day storm. *Journal of Geophysical Research: Space Physics*, *121*, 11,213–11,234. https://doi.org/10.1002/2016JA023165

Hashimoto, K. K., Kikuchi, T., Tomizawa, I., & Nagatsuma, T. (2017). Substorm overshielding electric field at low latitude on the nightside as observed by the HF Doppler sounder and magnetometers. *Journal of Geophysical Research: Space Physics*, *122*, 10,851–10,863. https://doi.org/10.1002/2017JA024329

Heelis, R. A. (1984). The effects of interplanetary magnetic field orientation on dayside high-latitude ionospheric convection. *Journal of Geophysical Research*, *89*(A5), 2873–2880. https://doi.org/10.1029/JA089iA05p02873

Huang, C.-S. (2009). Eastward electric field enhancement and geomagnetic positive bay in the dayside low-latitude ionosphere caused by magnetospheric substorms during sawtooth events. *Geophysical Research Letters*, *36*, L18102. https://doi.org/10.1029/2009GL040287

Huang, C.-S. (2012). Statisticala nalysis of dayside equatorial ionospheric electric fields and electrojet currents produced by magnetospheric substorms during sawtooth events. *Journal of Geophysical Research*, *117*, A02316. https://doi.org/10.1029/2011JA017398

Huang, C.-S., Foster, J. C., Goncharenko, L. P., Reeves, G. D., Chau, J. L., Yumoto, K., & Kitamura, K. (2004). Variations of low-latitude geomagnetic fields and Dst index caused by magnetospheric substorms. *Journal of Geophysical Research*, *109*, A05219. https://doi.org/10.1029/2003JA010334

Huang, C. S., Foster, J. C., & Kelley, M. C. (2005). Long-duration penetration of the planetary electric field to the low-altitude ionosphere during the main phase of magnetic storms. *Journal of Geophysical Research*, *110*, A11309. https://doi.org/10.1029/2005JA011202

Huang, C.-S., Wilson, G. R., Hairston, M. R., Zhang, W. W., & Liu, J. (2016). Equatorial ionospheric plasma drifts and O^+ concentration enhancements associated with disturbance dynamo during the 2015 St. Patrick's Day magnetic storm. *Journal of Geophysical Research: Space Physics*, *121*, 7961–7973. https://doi.org/10.1002/2016JA023072

Huang, C.-S., Yumoto, K., Abe, S., & Sofko, G. (2008). Low-latitude ionospheric electric and magnetic field disturbances in response to solar wind pressure enhancements. *Journal of Geophysical Research*, *113*, A08314. https://doi.org/10.1029/2007JA012940

Iijima, T., Fujii, R., Potemra, T. A., & Saflekos, N. A. (1978). Field-aligned currents in the south polar cusp and their relationship to the interplane- tary magnetic field. *Journal of Geophysical Research*, *83*, 5595.

Iijima, T., & Potemra, T. A. (1976). Field-aligned currents in the dayside cusp observed by Triad. *Journal of Geophysical Research*, *81*, 5971.

Kamide, Y., & Kusano, K. (2015). No major solar flares but the largest geomagnetic storm in the present solar cycle. *Space Weather*, *13*, 365–367. https://doi.org/10.1002/2015SW001213

Kane, R. P. (1974). Relation between the strength of the Sq current system and its focus position. *Proceedings of the Indian Academy of Sciences - Section A*, *A80*, 17–25.

Kelley, M. C., Fejer, B., & Gonzales, C. (1979). An explanation for anomalous equatorial ionospheric electric fields associated with a northward turning of the interplanetary magnetic field. *Geophysical Research Letters*, *6*, 301–304.

Kelley, M. C., & Makela, J. J. (2002). *By* dependent prompt penetrating electric fields at the magnetic equator. *Geophysical Research Letters*, *29*(7), 1153. https://doi.org/10.1029/2001GL014468

Kikuchi, T., & Araki, T. (1985). Preliminary positive impulse of geomagnetic sudden commencement observed at dayside middle and low latitudes. *Journal of Geophysical Research*, *90*, 12,195–12,200.

Kikuchi, T., Hashimoto, K. K., Kitamura, T. I., Tachihara, H., & Fejer, B. J. (2003). Equatorial counterelectrojets during substorms. *Journal of Geophysical Research*, *108*(A11), 1406. https://doi.org/10.1029/2003JA009915

Kikuchi, T., Hashimoto, K. K., & Nozaki, K. (2008). Storm phase dependence of penetration of magnetospheric electric fields to middle and low latitudes. In P. M. Kintner, et al. (Eds.), *Midlatitude Ionospheric Dynamics and Disturbances* (Chap. 2, pp. 145–155). Washington, DC: American Geophysical Union. https://doi.org/10.1029/181GM14

Kikuchi, T., Luhr, H., Kitamura, T., Saka, O., & Schlegel, K. (1996). Direct penetration of the polar electric fields to the equator during a DP 2 event as detected by the auroral and equatorial magnetometer chains and the EISCAT radar. *Journal of Geophysical Research*, *101*, 17,161–17,173.

Kikuchi, T., Luhr, H., Schlegel, K., Tachihara, H., Shinohara, M., & Kitamura, T. L. (2000). Penetration of auroral electric fields to the equator during a substorm. *Journal of Geophysical Research*, *105*, 23,251–23,261.

Kikuchi, T., Tsunomura, S., Hashimoto, K., & Nozaki, K. (2001). Fieldaligned current effects on midlatitude geomagnetic sudden commencements. *Journal of Geophysical Research*, *106*, 15,555–15,566.

Lopez, R. E., Wiltberger, M., Hernandez, S., & Lyon, J. G. (2004). Solar wind density control of energy transfer to the magnetosphere. *Geophysical Research Letters*, *31*, L08804. https://doi.org/10.1029/2003GL018780

Mannucci, A. J., Tsurutani, B. T., Iijima, B. A., Komjathy, A., Saito, A., Gonzalez, W. D., et al. (2005). Dayside global ionospheric response to the major interplanetary events of October 29-30, 2003 "Halloween Storms". *Geophysical Research Letters*, *32*, L12S02. https://doi.org/10.1029/2004GL021467

Nava, B., Rodríguez-Zuluaga, J., Alazo-Cuartas, K., Kashcheyev, A., Migoya-Orué, Y., Radicella, S. M., et al. (2016). Middle- and low-latitude ionosphere response to 2015 St. Patrick's Day geomagnetic storm. *Journal of Geophysical Research: SpacePhysics*, *121*, 3421–3438. https://doi.org/10.1002/2015JA022299

Nishida, A. (1968). Coherence of geomagnetic DP2 fluctuations with interplanetary magnetic variations. *Journal of Geophysical Research*, *73*, 5549–5559. https://doi.org/10.1029/JA073i017p05549

Nosé, M., Iyemori, T., Takeda, M., Toh, H., Ookawa, T., Cifuentes-Nava, G., et al. (2009). New substorm index derived from high-resolution geomagnetic field data at low latitude and its comparison with AE and ASY indices, in Proceedings of XIIIth IAGA Workshop on Geomagnetic Observatory Instruments, Data Acquisition, and Processing, U.S.Geol. Surv. Open File Rep., 2009–1226, edited by J. J. Love, pp. 202–207.

Nosé, M., Iyemori, T., Wang, L., Hitchman, A., Matzka, J., Feller, M., et al. (2012). Wpindex: A new substorm index derived from high-resolution geomagnetic field data at low latitude. *Space Weather*, *10*, S08002. https://doi.org/10.1029/2012SW000785

Rastogi, R. G. (1977). Geomagnetic storms and electric fields in the equatorial ionosphere. *Nature*, *268*, 422–424. https://doi.org/10.1038/268422a0

Rastogi, R. G., Chandra, H., & James, M. E. (1996). Nocturnal variations of geomagnetic horizontal field at equatorial stations. *Geophysical Research Letters*, *23*(19), 2601–2604. https://doi.org/10.1029/96GL02390

Rastogi, R. G., & Patel, V. L. (1975). Effect of interplanetary magnetic field on ionosphere over the magnetic equator. *Proceedings of the Indian Academy of Sciences - Section A*, *82A*, 121–141.

Reddy, C. A. (1989). The equatorial electrojet. *Pure and Applied Geophysics*, *131*, 485–508. https://doi.org/10.1007/BF00876841

Reeves, G., Henderson, M. G., Skoug, R. M., Thomsen, M. F., Borovsky, J. E., Funsten, H. O., et al. (2003). IMAGE, POLAR, and geosynchronous observations of substorm and ring current ion injection. In *Disturbances in geospace: The storm-substorm relationship* Geophys. Monogr. Ser. (Vol. *142*, pp. 91–101). Washington, DC: American Geophysical Union. https://doi.org/10.1029/142GM09

Rout, D., Chakrabarty, D., Sekar, R., Reeves, G. D., Ruohoniemi, J. M., Pant, T. K., et al. (2016). An evidence for prompt electric field disturbance driven by changes in the solar wind density under northward IMF *Bz* condition. *Journal of Geophysical Research: Space Physics*, *121*, 4800–4810. https://doi.org/10.1002/2016JA022475

Rudeout, W., & Coster, A. (2006). Automated GPS processig for global total electron content data. *GPS Solutions*, *10*(3), 219–228. https://doi.org/10.1007/s10291-006-0029-5

Ruohoniemi, J. M., & Greenwald, R. A. (2005). Dependencies of high-latitude plasma convection: Consideration of interplanetary magnetic field, seasonal, and universal time factors in statistical patterns. *Journal of Geophysical Research*, *110*, A09204. https://doi.org/10.1029/2004JA010815

Sastri, J., Rao, J., Rao, D., & Pathan, B. (2001). Daytime equatorial geomagnetic H field response to the growth phase and expansion phase onset of isolated substorms: Case studies and their implications. *Journal of Geophysical Research*, *106*, 29,925–29,933. https://doi.org/10.1029/2001JA900120

Sastri, J. H., Rao, J. V. S. V., & Ramesh, K. B. (1993). Penetration of polar electric fields to the nightside dip equator at times of geomagnetic sudden commencements. *Journal of Geophysical Research*, *98*, 17,517–17,523.

Scherliess, L., & Fejer, B. G. (1997). Storm time dependence of equatorial disturbance dynamo zonal electric fields. *Journal of Geophysical Research*, *102*, 24,037–24,046.

Senior, C., & Blanc, M. (1984). On the control of magnetospheric convection by the spatial distribution of ionospheric conductivities. *Journal of Geophysical Research*, *89*, 261–284. https://doi.org/10.1029/JA089iA01p00261

Spiro, R. W., Wolf, R. A., & Fejer, B. G. (1988). Penetration of high latitude electric field effects to low latitudes during SUNIDAL 1984. *Annales de Geophysique*, *6*(1), 39–50.

Tanaka, T. (2007). Magnetosphere-ionosphere convection as a compound system. *Space Science Reviews*, *133*(1), 1–72. https://doi.org/10.1007/s11214-007-9168-4

Thébault, E., Finlay, C. C., Beggan, C. D., Alken, P., Aubert, J., Barrois, O., et al. (2015). International Geomagnetic Reference Field: the twelfth generation. *Earth, Planets and Space*, *67*(1), 79. https://doi.org/10.1186/s40623-015-0228-9

Titheridge, J. E. (1995). Winds in the ionosphere—A review. *Journal of Atmospheric and Terrestrial Physics*, *57*, 1681–1714.

Tulasi Ram, S., RamaRao, P. V. S., Prasad, D. S. V. V. D., Niranjan, K., GopiKrishna, S., Sridharan, R., & Ravindran, S. (2008). Local time dependent response of post-sunset ESF during geomagnetic storms. *Journal of Geophysical Research*, *113*, A07310. https://doi.org/10.1029/2007JA012922

Tulasi Ram, S., Yokoyama, T., Otsuka, Y., Shiokawa, K., Sripathi, S., Veenadhari, B., et al. (2015). Duskside enhancement of equatorial zonal electric field response to convection electric fields during the St. Patrick's Day storm on 17 March 2015. *Journal of Geophysical Research: Space Physics*, *121*, 538–548. https://doi.org/10.1002/2015JA021932

Venkatesh, K., Patra, A. K., Balan, N., Fagundes, P. R., Tulasi Ram, S., Batista, I. S., & Reinisch, B. W. (2019). Superfountain effect linked with 17 March 2015 geomagnetic storm manifesting distinct F3 layer. *Journal of Geophysical Research: Space Physics*, *124*. https://doi.org/10.1029/2019JA026721

Venkatesh, K., Tulasi Ram, S., Fagundes, P. R., Seemala, G. K., & Batista, I. S. (2017). Electrodynamic disturbances in the Brazilian equatorial and low-latitude ionosphere on St. Patrick's Day storm of 17 March 2015. *Journal of Geophysical Research: Space Physics*, *122*, 4553–4570. https://doi.org/10.1002/2017JA024009

Wei, Y., Wan, W., Zhao, B., Hong, M., Ridley, A., Ren, Z., et al. (2012). Solar wind density controlling penetration electric field at the equatorial ionosphere during a saturation of cross polar cap potential. *Journal of Geophysical Research*, *117*, A09308. https://doi.org/10.1029/2012JA017597

Zhang, S.-R., Erickson, P. J., Zhang, Y., Wang, W., Huang, C., Coster, A. J., et al. (2017). Observations of ion neutral coupling associated with strong electrodynamic disturbances during the 2015 St. Patrick's Day storm. *Journal of Geophysical Research: Space Physics*, *122*, 1314–1337. https://doi.org/10.1002/2016JA023307

Zong, Q.-G., Reinisch, B. W., Song, P., Wei, Y., & Galkin, I. A. (2010). Dayside ionospheric response to the intense interplanetary shocks-solar wind discontinuities: Observations from the digisonde global ionospheric radio observatory. *Journal of Geophysical Research*, *115*, A06304. https://doi.org/10.1029/2009JA014796